Received: 28 December 2023 | Revised: 13 February 2024 | Accepted: 17 February 2024

DOI: 10.1111/mmi.15247

RESEARCH ARTICLE

WILEY

# The swimming defect caused by the absence of the transcriptional regulator LdtR in *Sinorhizobium meliloti* is restored by mutations in the motility genes *motA* and *motS*

**Richard C. Sobe** | **Birgit E. Scharf**

Department of Biological Sciences, Life Sciences I, Virginia Tech, Blacksburg, Virginia, USA

**Correspondence**
Birgit E. Scharf, Biological Sciences, Life Sciences I, Virginia Tech, Blacksburg, VA 24061, USA.
Email: bscharf@vt.edu

**Funding information**
National Science Foundation, Grant/Award Number: MCB-1817652 and MCB-2128232

## Abstract

The flagellar motor is a powerful macromolecular machine used to propel bacteria through various environments. We determined that flagellar motility of the alphaproteobacterium *Sinorhizobium meliloti* is nearly abolished in the absence of the transcriptional regulator LdtR, known to influence peptidoglycan remodeling and stress response. LdtR does not regulate motility gene transcription. Remarkably, the motility defects of the Δ*ldtR* mutant can be restored by secondary mutations in the motility gene *motA* or a previously uncharacterized gene in the flagellar regulon, which we named *motS*. MotS is not essential for *S. meliloti* motility and may serve an accessory role in flagellar motor function. Structural modeling predicts that MotS comprised an N-terminal transmembrane segment, a long-disordered region, and a conserved β-sandwich domain. The C terminus of MotS is localized in the periplasm. Genetics based substitution of MotA with $MotA_{G12S}$ also restored the Δ*ldtR* motility defect. The $MotA_{G12S}$ variant protein features a local polarity shift at the periphery of the MotAB stator units. We propose that MotS may be required for optimal alignment of stators in wild-type flagellar motors but becomes detrimental in cells with altered peptidoglycan. Similarly, the polarity shift in stator units composed of MotB/$MotA_{G12S}$ might stabilize its interaction with altered peptidoglycan.

**KEYWORDS**
bacterial flagella, peptidoglycan, rotary motor, suppressor mutations, swimming motility

## 1 | INTRODUCTION

The bacterial flagellum is a highly complex rotary machine that requires the activity of about 50 different protein products for its synthesis, regulation, and function (Galibert et al., 2001). Each flagellar filament alone consists of about 20,000 proteins. Thus, the flagellum-encoding genes are tightly regulated in a hierarchical fashion (Morimoto & Minamino, 2014). Motility gene regulation in the soil bacterium *Sinorhizobium meliloti* occurs in a three-tiered system controlled at its apex by products of the class IA genes *visN* and *visR*, which encode the LuxR-type global transcriptional regulators, VisN and VisR, named for being *vi*tal for *s*wimming (Sourjik et al., 2000). VisNR are constitutively produced, but only activate transcription of the class IB gene, *rem*, during exponential growth (Rotter et al., 2006; Sourjik et al., 2000). *rem* encodes the *r*egulator of *e*xponential growth *m*otility (Rem), an OmpR-like master regulator

that directly influences its own transcription in addition to activating class IIA (flagellar basal body) and class IIB (motor) gene transcription. Following assembly of the basal body, rod, and hook structures, class III genes, including those coding for flagellin and chemotaxis proteins, are activated in a manner dependent on the uncharacterized protein Orf38, the flagellin regulator FlbT, and the flagellar C-ring component FliM (Rotter et al., 2006).

Flagellum biosynthesis is initiated by assembly of the flagellar type 3 secretion system (fT3SS) and the MS ring, which surrounds the secretion system in the inner membrane (Johnson et al., 2021). The fT3SS serves as a portal for secretion of the main axial components, namely the rod, hook, and filament structures, as well as associated adaptor proteins (Johnson et al., 2021). The MS ring serves as a scaffold onto which the cytoplasmic C ring assembles and as an adapter for the transmission of torque from the C ring to the flagellar rod in the periplasm. The C ring comprised FliG, FliM, and FliN, influences flagellar rotation in response to chemotactic signals (Kinoshita et al., 2018; Sarkar et al., 2010). The flagellar rod is built atop the MS ring and protrudes through the periplasm, peptidoglycan layer, and the outer membrane. During rod formation, the peptidoglycan-associated P-ring component FlgI and lipopolysaccharide-associated L-ring component FlgH are secreted through the general secretion (SEC-dependent) pathway and assemble to form a fused bushing structure through which the rod rotates (Kaplan et al., 2019). The flexible hook (FlgE) is produced next and serves as a universal joint to permit the smooth transmission of rotary torque from the rod to the long (two to several micrometer) rigid flagellar filament as the motor rotates (Berg, 2003). Various transcriptional, post-transcriptional, and post-translational mechanisms are employed by bacteria to prevent the production of the hook-associated proteins, flagellins, flagellar cap, and associated chaperone proteins until assembly of the hook–basal body complex is completed (Ardissone & Viollier, 2015; Berg, 2003; Melamed et al., 2023). These mechanisms remain to be elucidated in *S. meliloti* but are hypothesized to include repression of flagellin gene transcription by the anti-σ factor FlbT, relief of FlbT-mediated repression by FlaF, and adjustment of fT3SS substrate specificity by the hook-associated protein chaperones FliJ and FliK and the flagellin chaperone FlaF as has been described for other bacteria that encode these proteins (Ardissone et al., 2020; Ferooz et al., 2011; Rotter et al., 2006; Tsang & Hoover, 2014; Zatakia et al., 2018).

Flagellar rotation is driven by the conversion of ion motive force into rotary motion by stator units comprising MotA and MotB for proton-driven stators or PomA and PomB for $Na^+$-driven stators (e.g., in *Vibrio* spp.), which are positioned as 11–16 studs in the inner membrane at the periphery of the basal body (Hu et al., 2021; Santiveri et al., 2020; Wadhwa & Berg, 2022). MotA consists of four transmembrane (TM) helices with a large cytoplasmic domain between TM2 and TM3, and a cytoplasmic C-terminal domain distal to TM4 (Blair & Berg, 1990). MotB consists of a short N-terminal stretch of amino acids in the cytoplasm followed by a TM domain and a periplasmic domain comprising a proton channel plug region, a linker region, and a peptidoglycan-binding domain (De Mot & Vanderleyden, 1994; Hosking et al., 2006; Kojima et al., 2018). Inactive stator complexes form in the inner membrane as a MotA pentamer surrounding a dimer of MotB (Deme et al., 2020; Santiveri et al., 2020; Wadhwa & Berg, 2022). Two proton channels formed between the TM helices of MotA and MotB are maintained in an inactive state by the MotB plug regions, which remain wedged within the crenellations formed by short periplasmic stretches of MotA (Tachiyama et al., 2022). This arrangement prevents unnecessary proton flow until the stators are activated by contact of MotA in free stators and the C-ring component FliG in the cytoplasm. Upon stator–rotor contact, the periplasmic regions of the MotB dimer extend upward to secure interactions between their OmpA/Pal-like peptidoglycan-binding domains and the rigid sacculus (Kojima et al., 2009, 2018; Morimoto et al., 2010; Roujeinikova, 2008; Van Way et al., 2000; Zhu et al., 2014). Consequently, the MotB proton plugs are released, the proton channels are opened, and proton flow through the stator units commences to drive rotation of the MotA ring around MotB (Wadhwa & Berg, 2022). This rotational energy is transmitted from MotA through interactions between MotA and FliG in the cytoplasmic C ring, which drives rotation of the entire basal body–hook–filament superstructure. Unlike the flagellar motors of many bacteria characterized to date, which rotate in one direction to drive swimming motility and reverse directions to cause cell tumbling and reorientation of swimming trajectories, *S. meliloti* motors rotate unidirectionally and are speed variable: its peritrichous flagella for a bundle when they rotate clockwise at the same speed during runs and reorientation events are initiated when one or more flagellar motors decelerate, causing asynchronization of filament rotation and splaying of the flagellar bundle (Scharf, 2002).

Peptidoglycan remodeling is a critical process in flagellum biosynthesis (Herlihey & Clarke, 2016). The rod, consisting of proximal rod (FliE, FlgB, FlgC, and FlgF) and distal rod (FlgG) substructures, spans the periplasm and must therefore pass through the peptidoglycan and outer membrane layers of the cell envelope (Johnson et al., 2021). As the average pore size of the peptidoglycan meshwork is about 2–4 nm and the rod diameter boasts about 10–20 nm, peptidoglycan remodeling is a necessary phase of rod synthesis. In some bacteria, including *Escherichia coli* and *Salmonella enterica*, peptidoglycan deconstruction required for rod insertion is catalyzed by the rod-associated FlgJ hydrolase, which caps the growing rod structure via its N-terminal rod-binding domain and contains a β-*N*-acetylglucosaminidase domain in its C-terminal region (Herlihey et al., 2014). Interestingly, in *Rhodobacter sphaeroides*, the functions of FlgJ are accomplished by two separate proteins: an $FlgJ_N$-like rod-binding protein and a lytic transglycosylase enzyme, SltF (García-Ramos et al., 2021; Herlihey & Clarke, 2016), and a similar arrangement has been observed for *S. meliloti* (Sobe et al., 2022). An appropriate peptidoglycan architecture is required for stator association with the peptidoglycan (Roure et al., 2012), which serves as a chassis within the cell envelope to stabilize the motor against the substantial forces required to drive flagellar filament rotation. MotB is predicted to bind reducing GlcNAc and/or nonreducing MurNAc and meso-diaminopimelic acid, similar to related OmpA

and Pal family proteins (Kojima et al., 2009; Roujeinikova, 2008; Roure et al., 2012). It has been proposed that OmpA-like domain proteins such as MotB bind to the peptidoglycan using a flexible clamp mechanism, which allows for dynamic associations of stators with the sacculus (Samsudin et al., 2016). Additionally, MotB has been shown to bind the NAM component of peptidoglycan directly (Roujeinikova, 2008).

Here, we have determined that the MarR-like transcriptional regulator, LdtR, known for its role in peptidoglycan remodeling and stress tolerance, is required for robust swimming motility. We determined that mutations in *motA* or the newly described gene *motS* restore motility to the Δ*ldtR* strain. Our data suggest that MotS may be involved in fine-tuning of stator alignment in the flagellar motor and high-velocity swimming of *S. meliloti*. RNA-seq analysis of the Δ*ldtR* strain compared to the wild type provides insights into potential mechanisms that cause motility disruption.

## 2 | RESULTS

### 2.1 | LdtR is required for full motility and osmotic stress tolerance but not synthesis of flagella in *S. meliloti*

To identify additional genes required for swimming motility in the wild-type *S. meliloti* strain RU11/001, we performed a mini-Tn5 transposon mutagenesis screen and screened for nonmotile mutants on soft-agar swim plates (Sobe et al., 2022). Sequencing the insertion sites after arbitrary-primed PCR amplifications of 41 transposants revealed that most mutants contained insertions in known flagellar genes or their promoters. However, one mutant harbored the transposon in gene locus SMRU11_37885 (*SMc01768* in strain 1021). To confirm that this gene contributes to flagellar motility, an unmarked in-frame deletion strain was constructed (BS244), which exhibited a 75% reduced swim ring when compared to wild type. This phenotype could be complemented to about 65% of wild-type levels by ectopic expression (Figure 1a).

SMRU11_37885 encodes a MarR-family transcriptional regulator, members of which usually serve roles in stress responses and neutralization or export of harmful compounds (Deochand & Grove, 2017; Nazaret et al., 2023). Pagliai et al. reported that the protein product, named LdtR for L,D-transpeptidase regulator, controls its own gene transcription, an adjacent gene encoding the L,D-transpeptidase, LdtP, and several other genes encoding peptidoglycan-modifying enzymes and small-molecule transporters in response to high osmotic stress (Pagliai et al., 2014, 2017). Additionally, mutants lacking either LdtR or LdtP showed reduced osmotic stress tolerance in *Liberibacter crescens* and *S. meliloti* strain 1021. We determined that the Δ*ldtR* mutant of *S. meliloti* strain RU11/001 exhibits similarly reduced osmotic stress tolerance in the presence of 0.5 M sucrose, which is restored upon ectopic complementation (Figure 1b).

The genes encoding the various structures of bacterial flagella are transcribed such that the structural components of the basal body are synthesized prior to initiating transcription of the highly abundant flagellin proteins that comprise flagellar filaments. This quality control ensures that copious levels of filament protein are only produced once a functional basal body is present on which to build the filament structure. Therefore, as an initial test to determine whether LdtR is involved in flagellar gene regulation, we compared the levels of flagellins for the wild-type and the Δ*ldtR* strain by immunoblot analysis (Figure 1c). We found no difference in the flagellin levels between these strains indicating that LdtR is unlikely to influence motility at the transcriptional level and that the main axial flagellar structures required for filament synthesis are properly assembled in the Δ*ldtR* mutant. Altogether, these data suggest that balanced levels of LdtR are important for osmotic stress tolerance and motility but not production of flagella in *S. meliloti*.

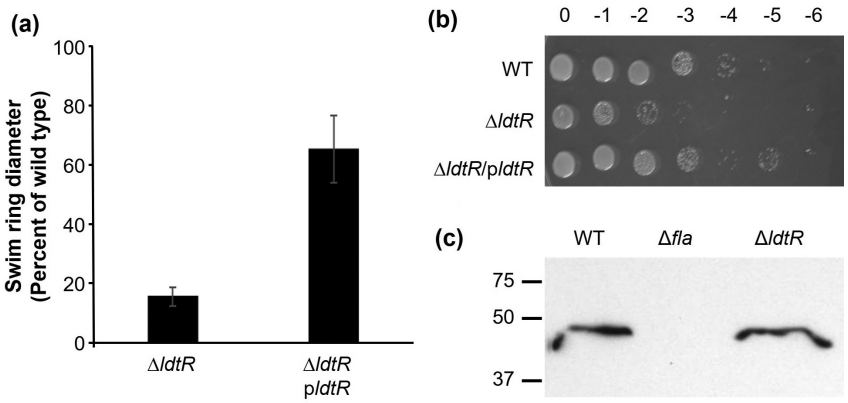


**FIGURE 1** Effects of the *ldtR* deletion on swim ring diameters, osmotic stress tolerance, and flagellation in *Sinorhizobium meliloti*. (a) Swim ring analysis of the Δ*ldtR* and complemented strains compared to wild type (WT). Shown are the averages and standard deviations of swim ring diameters for three independent experiments with three technical replicates each. (b) Representative osmotic stress tolerance assay of wild type, the Δ*ldtR*, and complemented strain on 0.5 M sucrose. The growth of all tested strains was indistinguishable on LB agar plates (data not shown). (c) Antiflagellin immunoblot analysis of wild type, Δ*fla* (negative control), and the Δ*ldtR* strain. Shown is a representative blot of three independent experiments.

## 2.2 | RNA-seq analysis reveals potential leads for mechanism of motility disruption in Δ*ldtR*

Previous RNA-seq reports indicated that chemical inactivation or changes in the cellular levels of LdtR caused dysregulation of various genes in *S. meliloti* and related organisms (Barnett et al., 2019; Pagliai et al., 2014, 2017). However, differential gene expression has not been analyzed for the Δ*ldtR* mutant and wild type. We compared global transcription levels of the Δ*ldtR* strain and *S. meliloti* wild type and identified genes with $Log_2$ fold ≥ ±1.0 fold change (i.e., twofold or greater altered regulation) and an adjusted *p* value of less than 0.05. The *S. meliloti* genome comprised a single circular chromosome, two large plasmids called pSymA and pSymB, and four smaller plasmids known as pSmeRU11a-d. Using these criteria, we identified 38 dysregulated genes on the chromosome and both large plasmids, with 30 of these being downregulated in the Δ*ldtR* strain indicating that LdtR serves primarily as a transcriptional activator (Table 1). The seven most downregulated genes were expressed between 16- and 5-fold less and include those coding for a transglutaminase, a GGDEF domain protein, a sigma 54-dependent Fis family transcriptional regulator, and four hypothetical proteins. BLASTP analysis of these hypothetical protein sequences provided top hits for Tad pilus proteins. Additional downregulated genes identified in the Δ*ldtR* mutant include genes encoding 13 proteins involved in small-molecule transport and metabolism, two glycosyl transferases, the GalE protein involved in LPS synthesis, an aminoacyl tRNA hydrolase, a PilZ domain protein likely to be involved in cyclic di-GMP-mediated regulation of cellular processes, and eight hypothetical proteins. Seven genes were upregulated in the Δ*ldtR* mutant compared to wild type and include those encoding an α/β hydrolase, four proteins involved in small-molecule transport and metabolism, an aminopeptidase, and one hypothetical protein. BLASTP analysis of the amino acid sequences of dysregulated genes that encode hypothetical proteins suggests that these proteins may include four associated with the Tad pilus, the CelJ cellulase, three involved with small-molecule transport, an HPE1-like plant virulence domain protein, an arginine *N*-methyltransferase, and three proteins with domains of unknown function including DUF995, DUF4168, and DUF5330. The genes identified in this screen that are most likely associated with peptidoglycan remodeling include the transglutaminase (SMRU11_36780), α/β hydrolase (SMRU11_33730), and the D-amino acid aminotransferase (SMRU11_09475). Additionally, *ldtP* (SMRU11_37880) transcription was only slightly altered with a nonsignificant increase of less than 10% in the Δ*ldtR* strain, suggesting that the motility defects observed for Δ*ldtR* are not caused by loss of LdtP production. Altogether, these results confirm that the motility defects observed in the Δ*ldtR* strain are not caused by disruptions in motility gene regulation but provide several alternative avenues to explain the motility phenotype including dysregulation of genes involved in peptidoglycan modification, cyclic di-GMP metabolism, and pilus assembly.

## 2.3 | Disruption of *motS* or alteration of the TM1-coding region of *motA* restores motility to the Δ*ldtR* mutant

Motility assays with the Δ*ldtR* strain on soft-agar swim plates revealed a robust tendency of this mutant to produce spontaneous suppressor mutations that result in strongly restored motility; about 60% of replicates assayed produced suppressor mutants within 4 days. The swim rings of these suppressor mutants are observed as flares arising at the perimeter of the parental mutant swim ring (Figure S1a). We isolated four independent suppressor mutants and quantified their swimming ability on soft-agar swim plates. All four mutants produced average swim ring diameters restored to about 65%–80% that of the wild type (Figure S1b). We also tested two suppressor mutants for osmotic stress tolerance and observed a very modest yet consistent improvement compared to the Δ*ldtR* parent strain on 0.5 M sucrose (Figure S1c) suggesting that the mechanism responsible for the decrease in motility and osmotic stress tolerance in the Δ*ldtR* mutant may be partially linked.

Whole-genome sequencing of four suppressor mutants revealed that three strains had acquired mutations in an uncharacterized gene, SMRU11_21380 (*Smc03025* in strain 1021). It is the 23rd gene in the contiguous flagellar regulon (Figure S2) located downstream of the gene encoding the flagellum-specific ATP synthase FliI and upstream of the gene encoding the flagellar basal body rod protein FlgB, and referred to hereafter as *motS* (Table 2). Mutations resulted in either a single amino acid substitution, P155L, the replacement of the last 16 aa with two non-native residues, or replacement of the last 71 aa with seven non-native residues (Figure S3). The fourth strain contained a mutation in the coding region for the motility protein MotA corresponding to a G12S amino acid substitution in the first transmembrane helix (Table 2). Deletion of *motS* or introduction of a $motA_{G12S}$ mutation in the Δ*ldtR* mutant by site-directed mutagenesis similarly restored motility to approximately 75% of the wild type, which confirmed that the mutations found in the suppressor mutants are indeed restoring motility (Figure 2 and Table 2). Comparable results were obtained for the Δ*ldtR* Δ*motS* $motA_{G12S}$ triple mutant indicating that the restorative effects of these mutations on the Δ*ldtR* strain are not additive. Notably, the $motA_{G12S}$ single mutant retained wild-type motility in this assay. The Δ*motS* mutant produced swim rings that were 75% of that of wild type.

## 2.4 | LdtR does not control cellular MotS levels or motility gene transcription

To determine whether the transcription factor LdtR regulates MotS production, we performed an immunoblot analysis with a MotS-specific polyclonal antibody and found no difference in the abundance of MotS in the Δ*ldtR* mutant compared to the wild type (Figure 3). Our RNA-seq analysis also revealed that the majority of motility genes were

**TABLE 1** Dysregulated genes in the Δ*ldtR* strain compared to wild type exceeding ±1.0 $Log_2$ fold change.

| Annotation | Locus tag | DE $Log_2$ ratio |
|---|---|---|
| Chromosome | | |
| Transglutaminase | SMRU11_36780 | −3.99 |
| Hypothetical protein (TadE/TadG pilus protein) | SMRU11_27440 | −3.98 |
| Sigma-54-dependent Fis family transcriptional regulator | SMRU11_27695 | −3.49 |
| GGDEF domain-containing protein | SMRU11_32230 | −2.35 |
| Hypothetical protein (TadG pilus protein) | SMRU11_32755 | −3.20 |
| Hypothetical (TadE/TadG pilus protein) | SMRU11_33790 | −2.16 |
| Hypothetical (TadG pilus protein) | SMRU11_33785 | −2.13 |
| Hypothetical (plant virulence factor HPE1-like domain) | SMRU11_20280 | −2.08 |
| 2-Oxoglutarate dehydrogenase subunit E1 | SMRU11_26310 | −1.36 |
| Malate dehydrogenase | SMRU11_26295 | −1.36 |
| Hypothetical (DUF5330) | SMRU11_19505 | −1.28 |
| Succinyl-CoA synthetase subunit alpha | SMRU11_26305 | −1.26 |
| Succinyl-CoA ligase subunit beta | SMRU11_26300 | −1.25 |
| Lysine transporter LysE | SMRU11_26320 | −1.20 |
| UDP-glucose 4-epimerase GalE | SMRU11_22155 | −1.13 |
| Dihydrolipoamide succinyltransferase | SMRU11_26315 | −1.12 |
| Hypothetical (arginine *N*-methyltransferase) | SMRU11_26325 | −1.09 |
| Oxidoreductase | SMRU11_26330 | −1.08 |
| Phosphoenolpyruvate carboxykinase | SMRU11_24910 | −1.04 |
| Aminoacyl-tRNA hydrolase | SMRU11_24905 | −1.03 |
| ATP-binding protein (PilZ domain) | SMRU11_34255 | −1.01 |
| DUF2312 | SMRU11_21960 | 1.02 |
| Alpha/beta hydrolase | SMRU11_33730 | 1.09 |
| pSymA | | |
| Aminopeptidase | SMRU11_09480 | 1.01 |
| D-amino acid aminotransferase | SMRU11_09475 | 1.15 |
| ABC transporter ATP-binding protein | SMRU11_09830 | 1.18 |
| ABC transporter substrate-binding protein | SMRU11_09835 | 1.34 |
| pSymB | | |
| Hypothetical protein (CelJ cellulase) | SMRU11_17900 | −3.66 |
| Hypothetical protein (DUF995 domain) | SMRU11_17905 | −2.37 |
| C4-dicarboxylate transporter DctA | SMRU11_12275 | −1.97 |
| Hypothetical (TctB family tricarboxylate transporter) | SMRU11_11880 | −1.42 |
| Hypothetical (tricarboxylate transporter substrate binding protein) | SMRU11_11885 | −1.31 |
| Autotransporter | SMRU11_14930 | −1.25 |
| Glycosyl transferase | SMRU11_13190 | −1.24 |
| Hypothetical (tricarboxylate transporter permease) | SMRU11_11875 | −1.13 |
| Glycosyl transferase | SMRU11_13200 | −1.08 |
| Guanine deaminase | SMRU11_15885 | 1.00 |
| Hypothetical (DUF4168) | SMRU11_13520 | 1.11 |

*Note*: Negative values indicate downregulation of the gene in Δ*ldtR* compared to wild type. For hypothetical proteins, top BLASTP hits are shown in parentheses.

Abbreviation: DE, differential expression.

not dysregulated (Table S2). Only four motility genes, *motB*, *flil* (coding for the fT3SS ATPase), *visN*, and $flgJ_C$ exhibited statistically significant reductions in gene transcription falling between −0.38 and −0.53 $Log_2$ fold change. Since flagellin synthesis is unaffected (Figure 1c), it is unlikely that these slightly decreased transcription levels adequately account for the severely reduced motility of the Δ*ldtR* mutant.

**TABLE 2** Locations and effects of mutations identified in Δ*ldtR* suppressor mutants from *Sinorhizobium meliloti* RU11/001.

| Mutant ID | Mutation | Protein effect |
|---|---|---|
| Suppressor 1 | $motS_{G502-}$ | Replacement of 16 aa with 2 aa |
| Suppressor 2 | $motS_{C464T}$ | $MotS_{P155L}$ |
| Suppressor 3 | *motS*::ISRm21 | Replacement of 71 aa with 7 aa |
| Suppressor 4 | $motA_{G34A}$ | $MotA_{G12S}$ |

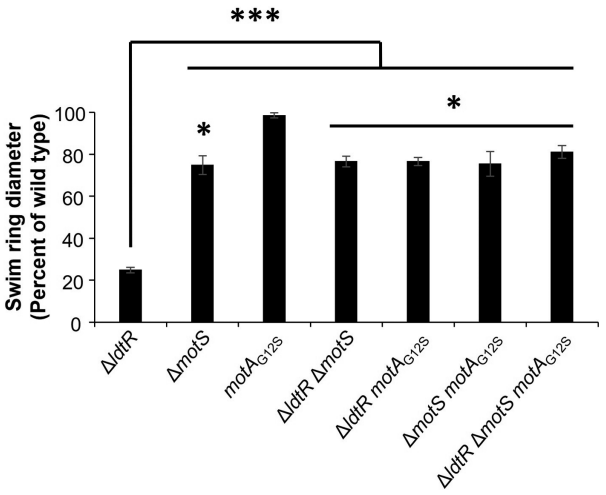


**FIGURE 2** Swim ring analysis of various mutants compared to wild type. Shown are the averages and standard deviations of swim ring diameters for three independent experiments with three technical replicates each. Asterisks indicate statistically significant differences between the indicated strain compared to wild type (*, $p < 0.05$) or Δ*ldtR* (***, $p < 0.0001$) as determined by one-way ANOVA.

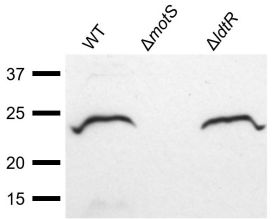


**FIGURE 3** Anti-MotS immunoblot analysis of cellular MotS levels in wild type (WT) and Δ*ldtR*. Shown is a representative blot of three independent experiments.

## 2.5 | The Δ*ldtR* population exhibits substantially reduced numbers of motile bacteria and reduced swimming velocities

To better understand how flagellar motility is affected by the loss of LdtR and its restorative mutations, we quantified the percentage of motile bacteria and their swimming velocities in liquid culture using phase-contrast microscopy. Wild-type, Δ*motS*, and $motA_{G12S}$ populations contained about 40%–50% motile bacteria (Figure 4a). In contrast, the percentage of motile bacteria in the Δ*ldtR* population was considerably reduced to just 4%. This phenotype was restored to wild-type levels in the double mutants Δ*ldtR* Δ*motS* and Δ*ldtR* $motA_{G12S}$. The *S. meliloti* wild type exhibited a swimming velocity of 40 μm/s, while the small population of motile Δ*ldtR* bacteria reached average velocities of less than 30 μm/s. The swimming velocities of Δ*motS* and Δ*ldtR* Δ*motS* were moderately reduced to just over 35 μm/s. Notably, the Δ*ldtR* $motA_{G12S}$ strain reached average velocities of less than 30 μm/s, whereas the $motA_{G12S}$ point mutant retained wild-type proficiency. These data indicate that the $MotA_{G12S}$ mutant protein is less capable of restoring physiological swimming speed defects caused by the loss of LdtR as compared to the removal of MotS.

Since LdtR plays a role in peptidoglycan remodeling, we hypothesized that the loss of LdtR may affect motility at higher viscosities by diminishing the ability of stators to remain bound to potentially suboptimal peptidoglycan binding sites in the Δ*ldtR* strain under high loads. We tested the swimming velocities of each strain in varying viscosities by adding Ficoll to concentrations of 5%, 10%, and 15%. All six strains exhibited consistent and proportionally decreased velocities as viscosity increased: the wild-type and $motA_{G12S}$ strains were the fastest, the Δ*motS* and Δ*ldtR* Δ*motS* strains were slightly slower, and the Δ*ldtR* and Δ*ldtR* $motA_{G12S}$ strains exhibited the slowest velocities at all Ficoll concentrations (Figure 4b). Statistically significant reductions in swimming velocity compared to wild type were observed for Δ*ldtR* and Δ*ldtR* $motA_{G12S}$ at 0%, 5%, and 10% Ficoll.

Altogether, these experiments revealed that the majority of the Δ*ldtR* population is nonmotile and the remaining motile cells exhibit impaired motility. The marginally diminished Δ*motS* motility phenotype is dominant over the absence of LdtR. The $MotA_{G12S}$ mutant protein restores the motile population in the absence of LdtR but does not restore the swimming velocity defect as effectively as a *motS* deletion. Finally, the small proportion of motile cells in the Δ*ldtR* population exhibits a consistently diminished swimming capacity under varying viscosities indicating that, once secured, stator interactions with the peptidoglycan are not perturbed under high loads.

## 2.6 | MotS is required for a narrowly focused range of flagellar motor rotation rates

Based on a search of the current BLAST records, the *motS* gene is confined to a small group of alphaproteobacteria including *Bradyrhizobium* sp. BRP14, *Ensifer aridi*, *Pararhizobium polonicum*, *Rhizobium herbae*, and *Shinella oryzae*, and its protein product has yet to be characterized. Notably, a multiple sequence alignment with MotS homologs from these organisms revealed that the C-terminal ~60 aa residues of the protein is very highly conserved (Figure S4). To better understand how MotS contributes to flagellar motility, we quantified and compared tethered cell rotation rates of wild type and the Δ*motS* strain in varying viscosities. Surprisingly, despite a consistently reduced average swimming velocity for this mutant compared to wild type, Δ*motS* in liquid medium alone exhibited a slight but statistically significant increase in average tethered cell rotation rates (14.7 ± 5.1 Hz) compared to the wild type (13.0 ± 4.73 Hz) and produced a slightly bimodal distribution of flagellar motor rotation

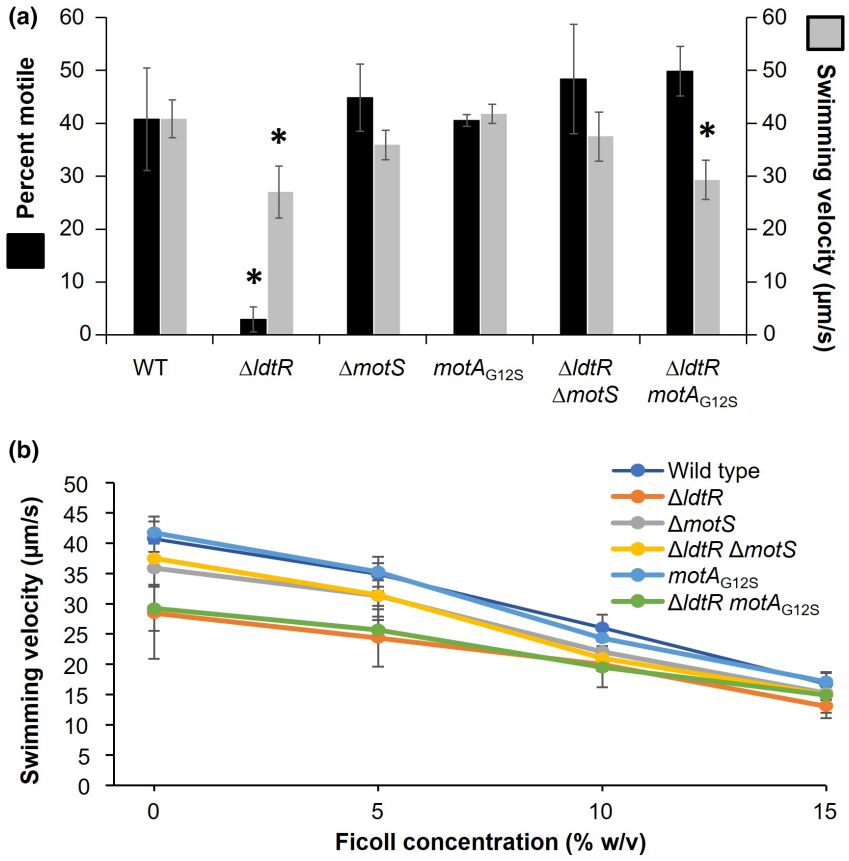


FIGURE 4 Quantification of swimming metrics for wild type (WT), Δ*ldtR*, and derivative strains in liquid medium. (a) Quantification of the percentage of motile bacteria and swimming velocities for Δ*ldtR* and second site mutant strains. The averages and standard deviations of data from three independent experiments with at least three videos per strain are reported. Asterisks indicate statistically significant differences between the indicated strain compared to wild type (*, $p < 0.05$) as determined by one-way ANOVA. (b) Quantification of swimming velocities in varying Ficoll concentrations. Statistically significant differences in velocity measurements were observed for Δ*ldtR* and Δ*ldtR motA*$_{G12S}$ compared to the wild type in 0%–10% Ficoll as determined by one-way ANOVA.

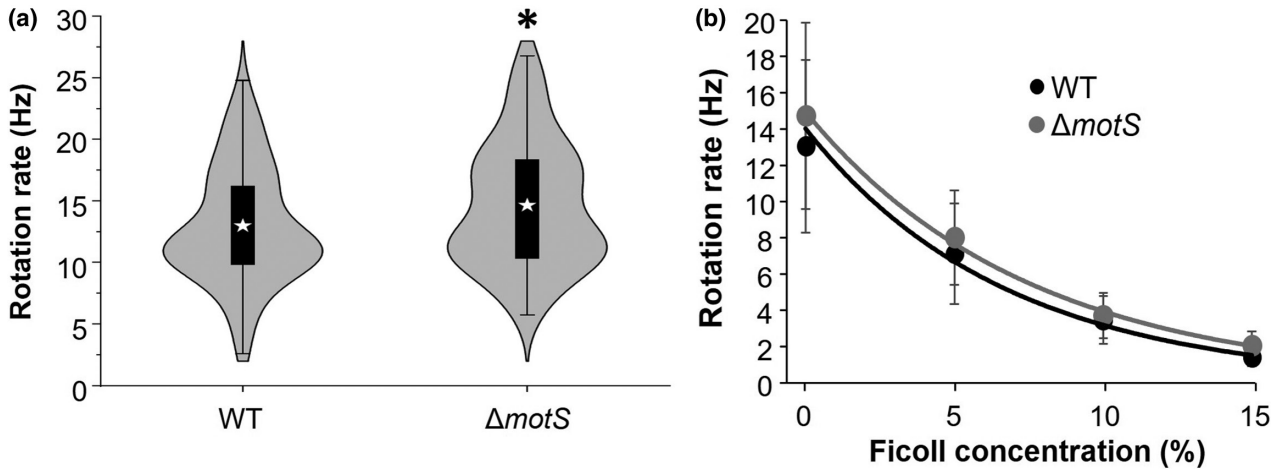


FIGURE 5 Quantification of tethered cell rotation rates for the Δ*motS* mutant compared to wild type (WT). (a) Violin plot depiction of tethered cell rotation rates for WT and Δ*motS* in motility medium lacking Ficoll. Stars mark the mean, boxes correspond to the interquartile range (IQR), and whiskers mark 1.5 IQR. The asterisk indicates a statistically significant difference from the wild type using the Student's *t* test ($p < 0.05$). (b) Tethered cell rotation rates in varying Ficoll concentrations. When possible, the same cells were identified, and rotation rates quantified for subsequent concentrations of Ficoll. Shown are averages and standard deviations of rotation rates for the following numbers of cells at different Ficoll concentrations: WT at 0%, $n = 75$; 5%, $n = 72$; 10%, $n = 65$, 15%, $n = 59$; Δ*motS* at 0%, $n = 75$; 5%, $n = 70$; 10%, $n = 66$; 15%, $n = 59$.

rates centered around 11.3 and 17.5 Hz (Figure 5a,b). Both strains showed proportionally equivalent reductions in rotation rates as viscosity increased (Figure 5b). These results suggest that MotS may be required for a narrowly focused range of flagellar motor rotation rates but does not impair the rotation of individual flagellar motors under high load.

## 2.7 | MotS contains a transmembrane domain near its N terminus and resides mainly in the periplasm

To gain insights into how disruption of *motS* could improve motility of the Δ*ldtR* strain, we investigated the cellular localization of MotS. The signal peptide prediction server SignalP 6.0 (Teufel et al., 2022) did

not identify a putative secretion signal peptide in MotS. Additionally, we detected MotS in cellular immunoblots near its predicted molecular weight of 20.4 kDa indicating that the protein is unlikely to be cleaved by signal peptidases (Figure 3). The TMHMM server (Krogh et al., 2001) predicted that MotS contains a short cytoplasmic domain (aa 1–25) followed by a transmembrane helix (aa 26–48) and a periplasmic domain (aa 49–183; Figure 6a). To experimentally validate these predictions, we employed the pKTop system, which drives production of a protein of interest fused at its C terminus to *E. coli* alkaline phosphatase (AP, encoded by *phoA*) and the alpha subunit of β-galactosidase (LacZα) (Karimova & Ladant, 2017). If the C terminus of MotS is located in the periplasm as predicted, PhoA will become activated, and an *E. coli* DH5α strain expressing the fusion protein will appear blue on indicator LB plates supplemented with the chromogenic alkaline phosphatase substrate X-Pho. Strains possessing a positive control plasmid encoding AP-LacZα fused to the C terminus of the outward-facing transmembrane domain of YmgF ($YmgF_{1-39}$) or unmodified pKTop negative control that encodes the cytoplasm-localized AP-LacZα fusion alone responded appropriately on indicator plates (Figure 6b). Bacteria producing the MotS-AP-LacZα fusion protein produced blue colonies on X-Pho plates, which indicates that the C-terminal region of MotS is located in the periplasm.

## 2.8 | MotS is predicted to possess a C-terminal β-sandwich domain similar to components of the type 2 secretion system and type 4 pilus

To investigate the putative structure of MotS, we submitted its amino acid sequence to AlphaFold Collab (Jumper et al., 2021). The results of this analysis suggested that the first 22 aa of MotS are disordered, followed by an alpha helix comprising aa 23–48, a long, disordered region with little predicted secondary structure from aa 50 to 127, and a β-sandwich domain from aa 128 to 183 (Figure 6c). Importantly, the predicted β-sandwich domain corresponds to the highly conserved C-terminal region revealed in the MotS multiple sequence alignment in Figure S4. We measured the length of the predicted MotS disordered periplasmic region in PyMol from the C-terminal point of the putative transmembrane helix to the N terminus of the sandwich domain to be approximately 16 nm. If this length were to protrude directly outward from the inner membrane toward

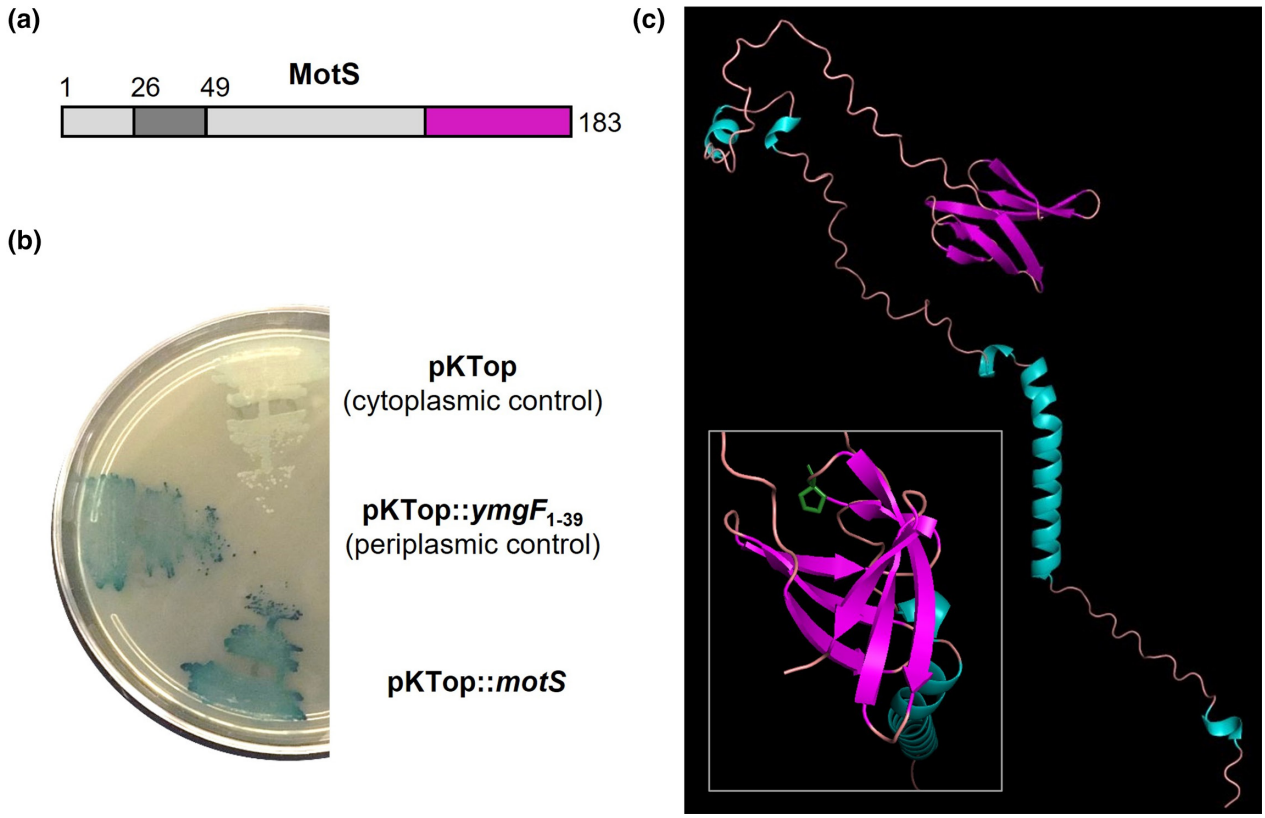


FIGURE 6 Membrane topology and structure prediction of MotS. (a) Schematic showing the predicted topology of MotS based on TMHMM analysis. Light gray, predicted disordered regions based on the AlphaFold prediction shown in (c); dark gray, transmembrane domain; magenta, periplasmic domain. (b) MotS membrane topology analysis by alkaline phosphatase (AP) reporter assay. *Escherichia coli* DH5α expressing unmodified AP (top), AP fused to the periplasmic control $YmgF_{1-39}$ (middle), or AP fused to MotS (bottom) were incubated on LB agar plates supplemented with X-Pho overnight at 30°C. Blue-colored bacterial colonies indicate periplasmic localization of the C terminus of the corresponding protein. (c) AlphaFold prediction of MotS structure. Cyan, alpha helix; magenta, beta sheet; peach, loop/disordered. The inset shows a top-down view of MotS with Pro-155, mutated to Leu in Suppressor 2, in green.

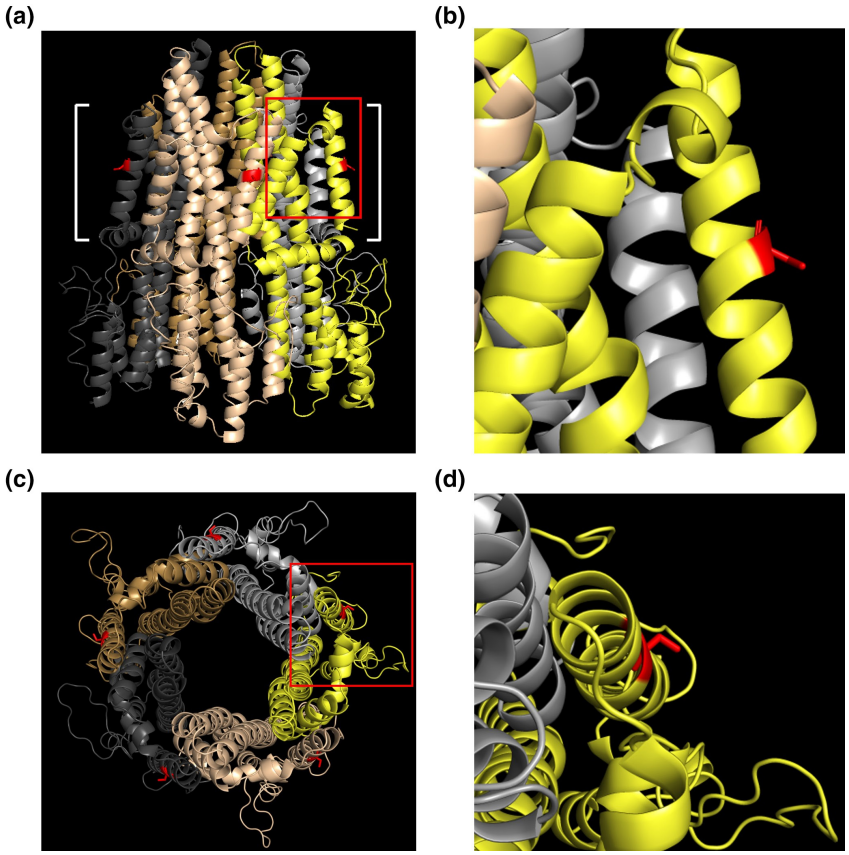


**FIGURE 7** Homology modeling and location of residue 12 in *Sinorhizobium meliloti* MotA. Side views (a and b) and top views (c and d) of the MotA pentamer showing the location of the G12S mutation (red) in each MotA chain. (b and d) are zoomed in images of the red boxed regions shown in (a and c), respectively. In (a), the membrane-embedded region of the MotA pentamer is indicated within white brackets.

the peptidoglycan and outer membrane, it would likely span much of the periplasmic space.

The Δ*ldtR* suppressor mutant analysis identified three mutations that caused a loss-of-function phenotype for MotS (Table 2). In two cases, disruption of *motS* by a frameshift mutation (Suppressor 1) or a transposon insertion (Suppressor 3) resulted in truncation of the MotS protein product by 16 aa or 79 aa, respectively, whereas the third mutation caused a single amino acid substitution (P155L, Suppressor 2). Notably, each of these mutations would have disruptive consequences for the putative β-sandwich domain (Figure 6 and Figure S3).

We submitted the MotS structure predicted by AlphaFold to the DALI server to identify proteins with similar structures. Top hits included the C-terminal globular domains of the enterotoxigenic *E. coli* type 2 secretion system (T2SS) protein GspC (PDB ID: 3OSS) and the type 4 secretion system (T4SS) protein PilP of *Pseudomonas aeruginosa* (PDB ID: 2Y4Y and 2LC4) and *Neisseria meningitidis* (PDB ID: 4AV2, Table S3). GspC serves to connect the T2SS assembly platform comprising GspF, GspL, and GspM in the inner membrane to a secretin channel formed by GspD in the outer membrane (Green & Mecsas, 2016; Py et al., 2001). PilP is part of the type 4 pilus (T4P) alignment complex and spans much of the periplasm to connect the T4P inner membrane complex and cytoplasmic ATPase assembly to the outer membrane complex (McCallum et al., 2019). Additionally, we submitted a sequence query to the SWISS-MODEL server, which resulted in a top hit for the Dot/Icm type 4 secretion system component DotF from *Legionella pneumophila* with an additional convincing hit for the *N. meningitidis* PilP protein (Table S4). DotF, along with DotG, is thought to form the periplasmic region of the T4SS and similarly connects inner and outer membrane components of the secretion system complex (Durie et al., 2020; Kubori et al., 2014). Together with the discovery that MotS is required for maximum swimming velocity and narrowly focused average motor rotation rates, we hypothesize that MotS serves a role in fine-tuning the alignment of stator units around the axial components of the *S. meliloti* flagellar motor.

## 2.9 | The $MotA_{G12S}$ substitution is predicted to affect the periphery of the MotA pentamer ring

To gain insights into how the $MotA_{G12S}$ mutant protein restores motility to the Δ*ldtR* mutant, we performed homology modeling mapping the location of the Gly12 residue of *S. meliloti* MotA using the recently solved *C. jejuni* $MotA_5MotB_2$ crystal structure (Santiveri et al., 2020) via the SWISS-MODEL server (Table S4). Gly12 is predicted to be positioned on the outside of the MotA pentamer ring about midway on TM1 of each monomer (Figure 7). Similar results were obtained when *S. meliloti* MotA was modeled to the recently solved *Bacillus subtilis* $MotA_5$ structure (Deme et al., 2020). The high GMQE, QMEANDisCo scores and coverage of these models suggest high confidence in the predicted location of the affected MotA residue. Therefore, the G12S substitution is projected to alter the local environment around flagellar stators within the inner membrane.

### 2.10 | Deletion of the peptidoglycan L,D-transpeptidase gene *ldtP* partially disrupts motility and deletion of *motS* exacerbates this effect

Previous research has shown that LdtR serves as a regulator of the peptidoglycan L,D-transpeptidase gene, *ldtP*, which is located immediately downstream of *ldtR* in the genomes of *S. meliloti* and related alphaproteobacteria including *Agrobacterium tumefaciens*, *L. crescens*, and *L. asiaticus* (Pagliai et al., 2014, 2017). Based on our findings that loss of LdtR causes motility defects and that MotS primarily resides in the periplasm and influences motor function, we hypothesized that peptidoglycan remodeling by LdtP may contribute to the observed motility defects. Therefore, we tested whether the Δ*ldtP* strain exhibits a motility defect similar to Δ*ldtR* and if subsequent deletion of *motS* mimicked the Δ*ldtR* Δ*motS* phenotype. The Δ*ldtP* mutation caused a modest 20% reduction in swimming motility on soft-agar swim plates, and the Δ*ldtP* Δ*motS* double mutant presented with a synergistic defect and swim ring diameters reaching 40% of wild type (Figure 8a). Combined with our RNA-seq data, these results suggest that the Δ*ldtR* motility phenotype and its restoration by inactivation of MotS is not attributable to loss of LdtP production.

### 2.11 | The osmotic stress tolerance defect in *ΔldtR* is marginally improved by deletion of *motS* but not by the *motA*$_{G12S}$ mutation

The Δ*ldtR* suppressor mutant analysis suggests that suppressor mutant strains S1 and S2 exhibit a partially restored osmotic stress defect compared to the Δ*ldtR* parent strain. To determine if the restorative mutations similarly improve osmotic stress tolerance of the Δ*ldtR* strain, we performed osmotic stress tolerance assays using LB agar plates supplemented with 0.5 M sucrose or 0.1% deoxycholate (Figure 8b). The Δ*motS* and *motA*$_{G12S}$ strains performed similar to wild type and the Δ*ldtR* strain showed reduced growth in the presence of both chemical treatments. Notably, the Δ*ldtR* Δ*motS* strain exhibited partially restored osmotic stress tolerance in the presence of both stressors that was more pronounced in the presence of deoxycholate, while the Δ*ldtR motA*$_{G12S}$ mutant performed similar to the Δ*ldtR* parent strain. In contrast to the Δ*ldtR* strain, Δ*ldtP* and Δ*ldtP* Δ*motS* strains showed no growth defect in the presence of deoxycholate or sucrose further indicating that under our assay conditions, the Δ*ldtR* motility and osmotic stress tolerance defects are not attributable to dysregulation of *ldtP*.

## 3 | DISCUSSION

In this work, we determined that the absence of the MarR-like transcriptional regulator LdtR causes a severe defect in *S. meliloti* motility but does not influence flagellar gene transcription. Remarkably, disruption of an otherwise dispensable flagellar protein, which we named MotS, caused a robust improvement in swimming motility of the Δ*ldtR* strain, as did replacing MotA with the MotA$_{G12S}$ variant. MotS is likely bound to the inner membrane and may span much of the periplasm. We hypothesize that MotS interacts via its predicted C-terminal β-sandwich domain with the peptidoglycan layer or other flagellar proteins to align and/or stabilize flagellar stators for optimal swimming performance. In the absence of LdtR, the presence of MotS apparently impedes motility but the Δ*ldtR* swimming defect can be similarly overcome by the presence of MotA$_{G12S}$ in stator units.

### 3.1 | The absence of LdtR severely impairs motility but not production of flagella

Multiple cellular pathways converge to influence *S. meliloti* flagellar motility at the transcriptional level. However, in each of these cases, motility gene regulation is exerted through modulation of *visNR* or *rem* transcription. Examples include the succinoglycan pathway controlled by ExoR, ExoS, and ChvI, the quorum sensing system SinI and ExpR, and the exopolysaccharide, motility, and membrane stress regulators

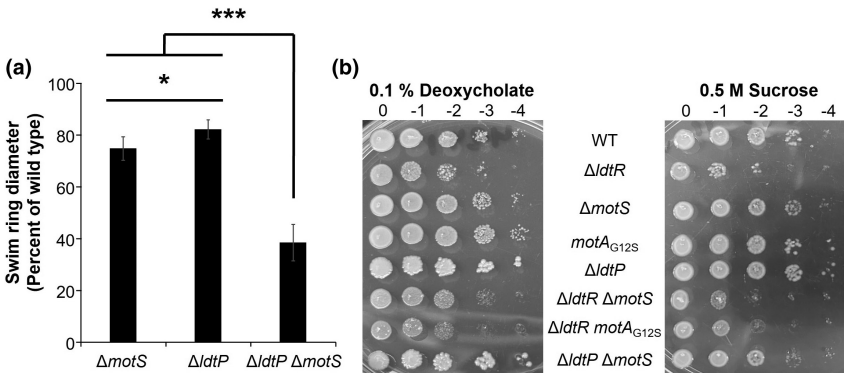


**FIGURE 8** Analysis of swimming proficiency and osmotic stress tolerance of *Sinorhizobium meliloti* wild type (WT) compared to mutant strains. (a) Quantification of swim ring diameters for Δ*ldtP* strains. Shown are the averages and standard deviations of swim ring diameters for three independent experiments with three technical replicates each. Asterisks indicate statistically significant differences between the indicated strain compared to wild type (*, $p < 0.05$) or Δ*ldtP* Δ*motS* (***, $p < 0.0001$) as determined by one-way ANOVA. (b) Representative osmotic stress tolerance assays for strains grown in the presence of 0.1% deoxycholate (left) and 0.5 M sucrose (right).

EmmABC, all of which negatively influence *visNR* transcription under specific environmental or physiological conditions. In contrast, the plant symbiosis regulator CbrA positively regulates *visNR* transcription, and the exopolysaccharide regulator MucR controls motility by repressing *rem* transcription (Scharf et al., 2016).

It has previously been proposed that the MarR-like transcriptional regulator LdtR controls motility in *S. meliloti* 1021 (Pagliai et al., 2017). In correlation with this notion, either loss of LdtR or its overproduction negatively impacted motility. However, in both circumstances, bacteria were reported to exhibit altered cellular morphology: a short-cell phenotype was described for the Δ*ldtR* mutant, while a strain that overexpressed *ldtR* was found to exhibit a branched cell morphology (Barnett et al., 2019). These phenotypes may be related to the abolished and enhanced activity of LdtR, as it has been directly linked to the transcriptional control of peptidoglycan modification and stress response genes (Barnett et al., 2019; Coyle et al., 2018; Loto et al., 2017; Padgett-Pagliai et al., 2022; Pagliai et al., 2014, 2017). Altered cell morphology in these strains is plausibly explained by disrupted peptidoglycan remodeling when LdtR levels are imbalanced, but it is unlikely that a shortened cell morphology is responsible for the extensive loss of motility presented by the *ldtR* deletion mutant that we report here. Immunoblot and RNA-seq analyses clearly showed that LdtR does not affect flagellum synthesis in *S. meliloti* RU11/001 (Figure 1c and Table 1), which, when combined with phenotypic data, suggest that the substantially reduced motility observed in the Δ*ldtR* strain is caused by a defect in flagellar motor function. Importantly, while the number of motile bacteria was decreased by about 15-fold in the Δ*ldtR* strain, the remaining population of motile bacteria were found to swim at velocities 30% slower than the wild type. Altogether, we conclude that when LdtR is absent, there is a substantially reduced probability that physiological conditions are appropriate to support motility.

### 3.2 | Removal of MotS or presence of $MotA_{G12S}$ restores motility to Δ*ldtR*

Suppressor mutant data demonstrated that the Δ*ldtR* motility defects were most readily overcome not only by disruption of the MotS globular domain but also by alteration of the membrane-proximal side chain composition of MotA. Based on these findings, an attractive explanation for the motility defect is that altered peptidoglycan remodeling in the Δ*ldtR* strain severely disrupts rotor–stator interactions. Notably, detection of wild-type flagellin levels in the Δ*ldtR* strain indicates that peptidoglycan remodeling necessary for production of the axial rod–hook–filament structure is not impeded. This observation infers that LdtR may play a role in mediating control of peptidoglycan remodeling necessary for (1) stator association with the peptidoglycan and/or (2) association of a stator alignment module with the sacculus.

Since MotS levels were comparable in wild type and the Δ*ldtR* strain, we conclude that the presence of MotS becomes detrimental for flagellar motor function in the absence of LdtR and propose that MotS may be involved in rotor–stator alignment. Notably, motility of the Δ*motS* strain was only slightly impaired, which indicates that the role of MotS in swimming motility is secondary and perhaps aimed toward fine-tuning of the rotor–stator arrangement to maximize power transfer. Biochemical and structure modeling data suggest that MotS is anchored in the inner membrane via a transmembrane domain with a disordered region approximately 15 nm in length and the C-terminal region (aa 128–183) forming a β-sandwich domain similar to the C-terminal domains of proteins involved in alignment of inner and outer membrane components of the T2SS (GspB/C), T4P (PilP), and Dot/Icm T4SS (DotF). Notably, GspB, GspC, PilP, and DotF proteins form part of a tube/ring structure in their respective macromolecular machines as do essentially all components of flagellum, pilus, and secretion systems (Durie et al., 2020; Green & Mecsas, 2016; Kubori et al., 2014; McCallum et al., 2019; Py et al., 2001; Wadhwa & Berg, 2022). Therefore, we speculate that MotS likely associates with the motor as one or more rings. It will be interesting to determine the exact location of MotS within the flagellar motor. In one feasible scenario, MotS surrounds the rod to position stators appropriately to promote maximum swimming velocity. Interestingly, a recent report describes the co-opting of the T4P components PilM, PilN, and PilO in the form of a cage structure around the flagellar motor in *Helicobacter pylori* (Liu et al., 2024). Notably, rather than improve motility as is the case for MotS in *S. meliloti*, the presence of these components caused diminished motility and a greater propensity to aggregate as compared to deletion mutants devoid of the corresponding genes. We hypothesize that MotS may be distantly related to PilP and adapted to serve roles in flagellar function. Additional flagellar motor substructures beyond those produced by *E. coli* and *S. enterica* have been identified in the form of various disks and rings in the close relative of *S. meliloti*, *R. sphaeroides*, as well as in *Vibrio* spp., *C. jejuni*, *B. subtilis*, *Borrelia burgdorferi*, and other species (Minamino & Imada, 2015; Terashima et al., 2017; Zhou & Roujeinikova, 2021). These are thought to serve stabilizing roles in their associated motors due to demands for higher swimming velocity or performance under high viscosity conditions. Thus, we anticipate that *S. meliloti* engages structural diversity compared to other systems to meet its need to power through the soil environment.

### 3.3 | Additional components required for the function of the *S. meliloti* flagellar motor

It has previously been suggested that *S. meliloti* requires relatively powerful flagellar motors to swim efficiently through its soil environment, a notion supported by the higher swimming velocities (~40 μm/s) observed here and previously (Attmannspacher et al., 2005; Götz & Schmitt, 1987; Sobe et al., 2022) compared to enteric counterparts such as *E. coli* (~25–30 μm/s), despite similar cell size, flagellar number, and organization (Albanna et al., 2018; Darnton et al., 2007; Kamdar et al., 2023). Various adaptations to the flagellar motors of diverse bacteria have been reported to meet the demand for greater flagellar motor power. These include increasing

the flow of protons through a given motor by increasing the number of stators situated around the rotor. Additionally, to accommodate a higher number of stators, the diameter of the stator ring around the basal body has been increased, which effectively lengthens the lever arm distance to provide additional power (Beeby et al., 2016; Deme et al., 2020; Minamino & Imada, 2015). Based on our data, we propose that MotS plays a role in increasing overall swimming speed or fine-tuning motor speed in *S. meliloti*.

We recently characterized the roles of *S. meliloti* FliL and its paralog MotF in stator function (Sobe et al., 2022). FliL is required for stator function and perhaps recruitment of stator elements to the basal body, while MotF appears to modulate the MotB proton plug. Both proteins were found to interact with one another as well as with both stator components, MotA and MotB. Additionally, we characterized additional periplasmic motor proteins MotC and its chaperone MotE, which are required for motility in *S. meliloti* (Eggenhofer et al., 2004; Platzer et al., 1997). The role of MotC remains elusive but is believed to interact with the stator protein MotB. Since MotS contains a transmembrane domain and resides mostly in the periplasm (Figures 4 and 5), we predict that it interacts with one or more of these additional components in the flagellar motors of *S. meliloti*. Our finding that the Δ*motS* mutant swims slightly slower than the wild type at varying viscosities, but that the tethered cell rotation rate profiles of these strains are comparable implies that MotS function may be less important or noticeable under high load.

Since flagellar genes were not dysregulated and flagellins were produced at wild-type levels in the Δ*ldtR* strain, the motility defect could be related to diminished torque transmission due to impaired stator alignment caused by a disruption of MotB binding to the peptidoglycan structure. Alternatively, placement of flagellar motor components involved in aligning stators with respect to the basal body could be affected. For example, the flagellar motors of *Vibrio fischeri* and *Campylobacter jejuni* require additional substructures not found in *E. coli* or *S. enterica* that are essential for stator recruitment in the flagellar motor (Beeby et al., 2016). In further support of this, replacement of wild-type MotA with the $MotA_{G12S}$ variant, which is predicted to alter the immediate environment surrounding stators in the inner membrane, restores swimming motility of the Δ*ldtR* strain similarly to removing MotS. We suspect that this altered environment displaces MotS in the motors and restores stator positioning with respect to the rotor. Notably, provision of $MotA_{G12S}$ in Δ*ldtR* does not restore the swimming velocities to the same degree as the removal of MotS indicating that the negative impact of MotS is not entirely restored when Δ*ldtR* motility is rescued by $MotA_{G12S}$. Alternative explanations for these findings include the possibility that the G12S substitution stabilizes cellular MotA and/or stator unit levels or partially neutralizes some as of yet unidentified inhibitors of stator incorporation. In the latter scenario, this player could well be MotS, which would explain the partial improvement of motility observed for the Δ*ldtR* $motA_{G12S}$ strain compared to Δ*ldtR* Δ*motS*. Cryo-electron tomography has not yet been performed to visualize the *S. meliloti* flagellar motor and would be a powerful tool in future work for verifying whether stator positioning is indeed affected by the removal of LdtR or MotS, or replacement of MotA with the $MotA_{G12S}$ variant protein in the Δ*ldtR* strain.

### 3.4 | Altered transcription of peptidoglycan-modification genes may explain the Δ*ldtR* phenotype

It has been shown previously that peptidoglycan-modifying enzymes, including the lytic transglycosylases Slt and MltD from *S. typhimurium* and the glucosaminidase Auto from *Listeria monocytogenes*, are required for flagellar motility (Herlihey & Clarke, 2016). Deletion of genes encoding any of these enzymes was determined to paralyze cells without impeding flagellar synthesis. Therefore, we suspected that deletion of *ldtR* caused dysregulation of the adjacent gene *ldtP*, which encodes an L,D-transpeptidase involved in peptidoglycan remodeling and has been shown to be regulated by LdtR (Coyle et al., 2018; Pagliai et al., 2014, 2017). However, RNA-seq results and the Δ*ldtP* and Δ*ldtP*Δ*motS* mutants motility and osmotic stress tolerance phenotypes reported here refute this hypothesis. Nonetheless, RNA-seq analysis revealed several dysregulated genes in the Δ*ldtR* strain that encode a transglutaminase (SMRU11_36780, 16-fold reduced), an uncharacterized hydrolase (SMRU11_33730) and a D-amino acid aminotransferase (SMRU11_09475) that will be investigated for roles in peptidoglycan synthesis and flagellar motility in future studies.

### 3.5 | Additional leads from RNA-seq to explain the Δ*ldtR* phenotype

Various strategies are used by bacteria to disable the function of intact flagella. In *R. sphaeroides*, one of the six CheY chemotaxis response regulators ($CheY_6$) directly binds to the cytoplasmic ring protein FliM to lock the rotor as a molecular brake during chemotaxis (Pilizota et al., 2009; Porter et al., 2006). In *B. subtilis*, the glycosyltransferase EpsE, required for exopolysaccharide synthesis during biofilm formation, also functions as a molecular clutch, which disengages flagellar stators from the rotor to prevent power transmission to flagella (Blair et al., 2008; Guttenplan et al., 2010). We identified two uncharacterized glycosyltransferases encoded by SMRU11_13190 and SMRU11_13200 that are located downstream of exopolysaccharide synthesis genes and were downregulated in Δ*ldtR* by >twofold. In addition to the molecular clutch, cyclic di-GMP-mediated inhibition of the stator component MotA has been described for *E. coli* (YcgR) and *B. subtilis* (YpfA) (Boehm et al., 2010; Fang & Gomelsky, 2010; Paul et al., 2010), and the cyclic di-GMP hydrolase BifA and synthase SadC increase and decrease flagellar motor reversals, respectively, in *P. aeruginosa* (Guttenplan & Kearns, 2013). We identified two strongly dysregulated genes (5.1-fold and 2.1-fold) in the Δ*ldtR* strain with putative roles in cyclic di-GMP sensing or metabolism (SMRU11_32230 and SMRU11_34255) that will be further investigated for possible roles in LdtR-dependent motility in future studies.

### 3.6 | Concluding remarks

The absence of LdtR in *S. meliloti* substantially reduces the population of motile cells. This motility defect can be restored by deletion of *motS* or by changing the peripheral transmembrane composition of MotA. MotS is a newly described motor component required for maximum swimming velocity and may contribute to stator positioning in wild-type motors. Intriguingly, its presence becomes detrimental in the absence of LdtR. Important questions remain including whether MotS is associated with the peptidoglycan and, if so, whether this occurs directly or through interactions with the P-ring protein FlgI or some as yet unidentified motor component(s). Additionally, which of the dysregulated genes identified in our RNA-seq analysis contributes to the Δ*ldtR* motility defect and how? Cryo-electron tomography studies will be invaluable for determining the precise localization of MotS as well as MotF and FliL, and potentially other as yet unidentified components in the speed-variable flagellar motor of *S. meliloti*.

## 4 | EXPERIMENTAL PROCEDURES

### 4.1 | Strains and plasmids

Derivative strains of *E. coli* K-12 and BL21 (DE3), highly motile derivatives of *S. meliloti* MVII-1, and plasmids used in this study are described in Table S1.

### 4.2 | Gene replacement and complementation

Mutant and plasmid-bearing *S. meliloti* strains were generated as described previously (Rotter et al., 2006).

### 4.3 | Media and growth conditions

*Escherichia coli* strains were routinely grown in lysogeny broth (LB; Bertani, 1951) at 37°C or 30°C supplemented with appropriate antibiotics at 100 μg/mL ampicillin (Ap) and 50 μg/mL kanamycin (Km). *Sinorhizobium meliloti* strains were routinely grown in tryptone–yeast extract–calcium chloride (TYC; 0.5% tryptone, 0.3% yeast extract, 0.087% $CaCl_2 \times H_2O$) broth supplemented with streptomycin (Sm) at 600 μg/mL at 30°C. Bromfield overlay plates were prepared by adding 12.5 mL Rhizobium basal medium (RB; 6.1 mM $K_2HPO_4$, 3.9 mM $KH_2PO_4$, 1 mM $MgSO_4$, 1 mM $(NH_4)_2SO_4$, 0.1 mM $CaCl_2$, 0.1 mM NaCl, 0.01 mM $Na_2MoO_4$, 0.001 mM $FeSO_4$, 20 mg/L biotin, and 100 mg/L thiamine) on Bromfield agar plates (0.04% tryptone, 0.01% yeast extract, 0.00067% $CaCl_2 \times H_2O$, 1.5% agar). Overlay plates were inoculated from TYC-Str culture with a starting $OD_{600}$ = 0.002 and grown at 30°C for 16 h to an $OD_{600}$ of 0.25 ± 0.05.

### 4.4 | Osmotic stress assays

*Sinorhizobium meliloti* strains were cultured for approximately 24 h in TYC-Sm at 30°C with agitation. TYC cultures were diluted to $OD_{600}$ = 0.002 in Bromfield overlay plate cultures and incubated at 30°C for approximately 17 h to an $OD_{600}$ = 0.2–0.3. Culture densities were normalized to $OD_{600}$ = 0.2, serially diluted prior to spot plating on LB plates containing 0.1% sodium deoxycholate or 0.5 M sucrose, and incubated for 4 days at 30°C.

### 4.5 | Swim plate assays

Stationary phase TYC-Str cultures were spot plated (3 μL) on Bromfield swim plates (containing 0.3% agar) and incubated at 30°C for 5 days for quantitative data or the indicated duration for qualitative images. Quantification of swim ring diameters reflect the averages and standard deviations of three independent experiments with three technical replicates each.

### 4.6 | Computerized motion analysis of swimming and tethered cells

Bacteria were prepared for swimming and tethered cell analysis as described previously (Sobe et al., 2022) with the following modifications. A 25% Ficoll-400 stock solution was dissolved in filtered overlay broth prepared as described Sobe et al. (2022). For swimming cell analysis, cultures standardized at an $OD_{600}$ = 0.2 were further diluted in an appropriate concentration of Ficoll-400 and filtered overlay broth to bring the final Ficoll concentration to 5%, 10%, or 15% and the final $OD_{600}$ to 0.04. For tethered cell analysis, tethered cells were imaged at 0% Ficoll concentration, and 400 μL of 5%, 10%, or 15% Ficoll in filtered overlay medium was carefully pipetted through the imaging chambers to replace the previous medium with the medium containing Ficoll. Stage graduations and microscopic imperfections on the glass coverslip were used to identify the exact locations videoed at 0% Ficoll to reimage the same cells at subsequent Ficoll concentrations.

### 4.7 | Purification of recombinant proteins

The periplasmic domain of MotS (MotS*) was expressed from pBS1331 in *E. coli* ER2566 (Table S1) and purified by Intein-Mediated Purification with an Affinity Chitin-binding Tag (IMPACT™) as described Sobe et al. (2022) with the following modifications. Cleavage of MotS* with dithiothreitol was performed for 40 hours at room temperature prior to eluting with IMPACT buffer at 4°C. The buffer used for preparative size exclusion chromatography consisted of 16.7 mM Tris/HCl, 125 mM NaCl, 10% glycerol, pH 7.5.

### 4.8 | Generation of the anti-MotS crude serum

MotS* was purified as described earlier and concentrated to 0.6 mg/mL using an Amicon ultrafiltration apparatus with a regenerated 10 kDa MWCO cellulose membrane. A total of 4.8 mg MotS* antigen was provided for polyclonal antibody production by Thermo Fisher Scientific.

### 4.9 | SDS-PAGE and immunoblotting

Aliquots (1 mL) of cultures grown in Bromfield overlay plates were harvested at 15,000*g*, all but ~15 μL of the supernatants were removed and suspended in 15 μL Laemmli buffer. Samples were boiled for 10 min. For flagellin immunoblots, 15 μL culture was mixed directly with Laemmli buffer and boiled for 10 min. Samples were stored at −20°C for at least 2 h prior to further processing. Immunoblot analyses were performed as described previously (Zatakia et al., 2018). Polyclonal anti-flagellin and anti-MotS crude sera were used at 1:10,000, and donkey anti-rabbit HRP secondary antibody (NA-934, Cytiva) was used at 1:1000.

### 4.10 | Membrane topology reporter assays

Membrane topology reporter assays used in this study employ a *phoA-lacZ*α transcriptional fusion to the 3′ end of *motS* in the pKTop plasmid to produce pBS1330 (Karimova et al., 2009; Karimova & Ladant, 2017). Strains with the positive control plasmid pBS1193 (producing $YmgF_{1\text{-}39}$-AP-LacZα) and negative control plasmid pKTop (producing AP-LacZα) were also used. Colonies of *E. coli* DH5α strains transformed with pKTop plasmids were streaked on LB agar supplemented with 1 mM IPTG, 80 μg/mL 5-chloro-4-bromo-3-indolyl phosphate (X-Pho) (RPI, Mt Prospect, IL, USA), and 50 μg/mL Km, and incubated for 18 h at 30°C.

### 4.11 | MotS and MotA structures modeling with AlphaFold and SWISS-MODEL

The MotS sequence was submitted to AlphaFold Colab, and both MotS and MotA were submitted to SWISS-MODEL using default parameters. The MotS structure predicted by AlphaFold Colab was submitted to the Dali server to identify similar protein structures from the full PDB database.

### 4.12 | RNA preparation, RNA sequencing, and transcriptomics analysis

Total RNA was isolated from wild type and Δ*ldtR* in three independent Bromfield overlay cultures grown to $OD_{600}$=0.20–0.25. Cultures were standardized to 2 mL at an $OD_{600}$ of 0.20, and RNA was extracted using the RNeasy Protect Bacteria Mini Kit (Qiagen) according to the manufacturer's protocol. RNA was stored at −80°C pending quality control analysis performed using aliquots of each sample. RNA integrity was verified by Agilent Tapestation analysis, and all samples had RIN values ≥9.3. DNA depletion was carried out using the RNase-Free DNase kit (Qiagen). For each sample, 1.25 μg total RNA per sample was provided for rRNA depletion with the Ribo-Zero™ Magnetic Kit (Epicenter), and libraries were prepared with the TruSeq Stranded mRNA library preparation kit (Illumina). Single-end sequencing was performed on a NextSeq 1000 flow cell with a 100-cycle sequencing module. Each sample was sequenced to a depth of 40–50 million reads. Onboard adapter trimming was performed, sequences were further quality trimmed using the BBDuk plugin in Geneious Prime® 2023.2.1 (http://www.geneious.com) with a base quality score cutoff of 20, and then filtered to remove sequences less than 30 nt. Cleaned reads were mapped to the *S. meliloti* RU11/001 genome (GenBank accession number GCA_001050915.2) in Geneious Prime® 2023.2.1 using the Geneious RNA mapper with default settings. Differential expression analysis was performed using the DESeqs2 plugin in Geneious Prime® 2023.2.1. Differentially expressed genes were filtered to include those with at least two fold change in expression and an adjusted $p<0.05$ for further analysis.

## AUTHOR CONTRIBUTIONS

**Birgit E. Scharf:** Conceptualization; funding acquisition; writing – original draft; writing – review and editing; project administration; resources; supervision; investigation; methodology. **Richard C. Sobe:** Conceptualization; investigation; writing – original draft; writing – review and editing; visualization; validation; methodology; software; formal analysis; project administration; data curation; supervision.

## ACKNOWLEDGMENTS

We thank the BIOL4644 class of 2017 for performing the transposon mutagenesis screen that identified the *ldtR* mutant motility defect. We thank Dr. Roderick Jensen for assistance with WGS analysis of the Δ*ldtR* suppressor mutants. We also thank Djelika Kabore and Parker Niccum for preliminary contributions to the swimming analysis of the Δ*ldtR* complemented strain and stress tolerance assays. The authors acknowledge funding from the National Science Foundation, Grant/Award Number: MCB-1817652 and MCB-2128232 to BES.

## CONFLICT OF INTEREST STATEMENT

The authors declare no conflict of interest.

## DATA AVAILABILITY STATEMENT

RNA-seq data are available at the Gene Expression Omnibus (GEO) database under accession number GSE251837 (https://www.ncbi.nlm.nih.gov/geo/query/acc.cgi?acc=GSE251837).

## ETHICS STATEMENT

No human or animal subjects were used in this work.

## ORCID

*Richard C. Sobe* https://orcid.org/0000-0003-2802-738X
*Birgit E. Scharf* https://orcid.org/0000-0001-6271-8972

## REFERENCES

Albanna, A., Sim, M., Hoskisson, P.A., Gillespie, C., Rao, C.V. & Aldridge, P.D. (2018) Driving the expression of the *Salmonella enterica* sv Typhimurium flagellum using flhDC from *Escherichia coli* results in key regulatory and cellular differences. *Scientific Reports*, 8, 16705.

Ardissone, S., Kint, N., Petrignani, B., Panis, G. & Viollier, P.H. (2020) Secretion relieves translational Co-repression by a specialized flagellin paralog. *Developmental Cell*, 55, 500–513.e4.

Ardissone, S. & Viollier, P.H. (2015) Interplay between flagellation and cell cycle control in *Caulobacter*. *Current Opinion in Microbiology*, 28, 83–92.

Attmannspacher, U., Scharf, B. & Schmitt, R. (2005) Control of speed modulation (chemokinesis) in the unidirectional rotary motor of *Sinorhizobium meliloti*. *Molecular Microbiology*, 56, 708–718.

Barnett, M.J., Solow-Cordero, D.E. & Long, S.R. (2019) A high-throughput system to identify inhibitors of Candidatus *Liberibacter asiaticus* transcription regulators. *Proceedings of the National Academy of Sciences of the United States of America*, 116, 18009–18014.

Beeby, M., Ribardo, D.A., Brennan, C.A., Ruby, E.G., Jensen, G.J. & Hendrixson, D.R. (2016) Diverse high-torque bacterial flagellar motors assemble wider stator rings using a conserved protein scaffold. *Proceedings of the National Academy of Sciences of the United States of America*, 113, E1917–E1926.

Berg, H.C. (2003) The rotary motor of bacterial flagella. *Annual Review of Biochemistry*, 72, 19–54.

Bertani, G. (1951) Studies on lysogenesis I: the mode of phage liberation by lysogenic *Escherichia coli*. *Journal of Bacteriology*, 62, 293–300.

Blair, D.F. & Berg, H.C. (1990) The MotA protein of *E. coli* is a proton-conducting component of the flagellar motor. *Cell*, 60, 439–449.

Blair, K.M., Turner, L., Winkelman, J.T., Berg, H.C. & Kearns, D.B. (2008) A molecular clutch disables flagella in the *Bacillus subtilis* biofilm. *Science*, 320, 1636–1638.

Boehm, A., Kaiser, M., Li, H., Spangler, C., Kasper, C.A., Ackermann, M. et al. (2010) Second messenger-mediated adjustment of bacterial swimming velocity. *Cell*, 141, 107–116.

Coyle, J.F., Pagliai, F.A., Zhang, D., Lorca, G.L. & Gonzalez, C.F. (2018) Purification and partial characterization of LdtP, a cell envelope modifying enzyme in *Liberibacter asiaticus*. *BMC Microbiology*, 18, 1–15.

Darnton, N.C., Turner, L., Rojevsky, S. & Berg, H.C. (2007) On torque and tumbling in swimming Escherichia coli. *Journal of Bacteriology*, 189, 1756–1764.

De Mot, R. & Vanderleyden, J. (1994) The C-terminal sequence conservation between OmpA-related outer membrane proteins and MotB suggests a common function in both gram-positive and gram-negative bacteria, possibly in the interaction of these domains with peptidoglycan. *Molecular Microbiology*, 12, 333–336.

Deme, J.C., Johnson, S., Vickery, O., Aron, A., Monkhouse, H., Griffiths, T. et al. (2020) Structures of the stator complex that drives rotation of the bacterial flagellum. *Nature Microbiology*, 5, 1553–1564.

Deochand, D.K. & Grove, A. (2017) MarR family transcription factors: dynamic variations on a common scaffold. *Critical Reviews in Biochemistry and Molecular Biology*, 52, 595–613.

Durie, C.L., Sheedlo, M.J., Chung, J.M., Byrne, B.G., Su, M., Knight, T. et al. (2020) Structural analysis of the *Legionella pneumophila* Dot/Icm type IV secretion system core complex. *eLife*, 9, e59530.

Eggenhofer, E., Haslbeck, M. & Scharf, B. (2004) MotE serves as a new chaperone specific for the periplasmic motility protein, MotC, in *Sinorhizobium meliloti*. *Molecular Microbiology*, 52, 701–712.

Fang, X. & Gomelsky, M. (2010) A post-translational, c-di-GMP-dependent mechanism regulating flagellar motility. *Molecular Microbiology*, 76, 1295–1305.

Ferooz, J., Lemaire, J. & Letesson, J.-J. (2011) Role of FlbT in flagellin production in *Brucella melitensis*. *Microbiology*, 157, 1253–1262.

Galibert, F., Finan, T.M., Long, S.R., Pühler, A., Abola, P., Ampe, F. et al. (2001) The composite genome of the legume symbiont *Sinorhizobium meliloti*. *Science*, 293, 668–672.

García-Ramos, M., de la Mora, J., Ballado, T., Camarena, L. & Dreyfus, G. (2021) Modulation of the enzymatic activity of the flagellar lytic transglycosylase SltF by rod components and the scaffolding protein FlgJ in *Rhodobacter sphaeroides*. *Journal of Bacteriology*, 203, e00372-00321.

Götz, R. & Schmitt, R. (1987) *Rhizobium meliloti* swims by unidirectional, intermittent rotation of right-handed flagellar helices. *Journal of Bacteriology*, 169, 3146–3150.

Green, E.R. & Mecsas, J. (2016) Bacterial secretion systems: an overview. *Microbiology Spectrum*, 4, 213–239.

Guttenplan, S.B., Blair, K.M. & Kearns, D.B. (2010) The EpsE flagellar clutch is bifunctional and synergizes with EPS biosynthesis to promote *Bacillus subtilis* biofilm formation. *PLoS Genetics*, 6, e1001243.

Guttenplan, S.B. & Kearns, D.B. (2013) Regulation of flagellar motility during biofilm formation. *FEMS Microbiology Reviews*, 37, 849–871.

Herlihey, F.A. & Clarke, A.J. (2016) Controlling autolysis during flagella insertion in gram-negative bacteria. *Protein Review*, 925, 41–56.

Herlihey, F.A., Moynihan, P.J. & Clarke, A.J. (2014) The essential protein for bacterial flagella formation FlgJ functions as a β-*N*-acetylglucosaminidase. *Journal of Biological Chemistry*, 289, 31029–31042.

Hosking, E.R., Vogt, C., Bakker, E.P. & Manson, M.D. (2006) The *Escherichia coli* MotAB proton channel unplugged. *Journal of Molecular Biology*, 364, 921–937.

Hu, H., Santiveri, M., Wadhwa, N., Berg, H.C., Erhardt, M. & Taylor, N.M. (2021) Structural basis of torque generation in the bi-directional bacterial flagellar motor. *Trends in Biochemical Sciences*, 47, 160–172.

Johnson, S., Furlong, E.J., Deme, J.C., Nord, A.L., Caesar, J.J., Chevance, F.F. et al. (2021) Molecular structure of the intact bacterial flagellar basal body. *Nature Microbiology*, 6, 712–721.

Jumper, J., Evans, R., Pritzel, A., Green, T., Figurnov, M., Ronneberger, O. et al. (2021) Highly accurate protein structure prediction with AlphaFold. *Nature*, 596, 583–589.

Kamdar, S., Ghosh, D., Lee, W., Tătulea-Codrean, M., Kim, Y., Ghosh, S. et al. (2023) Multiflagellarity leads to the size-independent swimming speed of peritrichous bacteria. *Proceedings of the National Academy of Sciences*, 120, e2310952120.

Kaplan, M., Ghosal, D., Subramanian, P., Oikonomou, C.M., Kjaer, A., Pirbadian, S. et al. (2019) The presence and absence of periplasmic rings in bacterial flagellar motors correlates with stator type. *eLife*, 8, e43487.

Karimova, G. & Ladant, D. (2017) Defining membrane protein topology using pho-lac reporter fusions. In: *Bacterial protein secretion systems*. New York, NY: Humana Press, pp. 129–142.

Karimova, G., Robichon, C. & Ladant, D. (2009) Characterization of YmgF, a 72-residue inner membrane protein that associates with the *Escherichia coli* cell division machinery. *Journal of Bacteriology*, 191, 333–346.

Kinoshita, M., Furukawa, Y., Uchiyama, S., Imada, K., Namba, K. & Minamino, T. (2018) Insight into adaptive remodeling of the rotor ring complex of the bacterial flagellar motor. *Biochemical and Biophysical Research Communications*, 496, 12–17.

Kojima, S., Imada, K., Sakuma, M., Sudo, Y., Kojima, C., Minamino, T. et al. (2009) Stator assembly and activation mechanism of the flagellar motor by the periplasmic region of MotB. *Molecular Microbiology*, 73, 710–718.

Kojima, S., Takao, M., Almira, G., Kawahara, I., Sakuma, M., Homma, M. et al. (2018) The helix rearrangement in the periplasmic domain of the flagellar stator B subunit activates peptidoglycan binding and ion influx. *Structure*, 26, 590–598.e5.

Krogh, A., Larsson, B., Von Heijne, G. & Sonnhammer, E.L. (2001) Predicting transmembrane protein topology with a hidden Markov model: application to complete genomes. *Journal of Molecular Biology*, 305, 567–580.

Kubori, T., Koike, M., Bui, X.T., Higaki, S., Aizawa, S.-I. & Nagai, H. (2014) Native structure of a type IV secretion system core complex essential for *Legionella* pathogenesis. *Proceedings of the National Academy of Sciences*, 111, 11804–11809.

Liu, X., Tachiyama, S., Zhou, X., Mathias, R.A., Bonny, S.Q., Khan, M.F. et al. (2024) Bacterial flagella hijack type IV pili proteins to control motility. *Proceedings of the National Academy of Sciences of the United States of America*, 121, e2317452121.

Loto, F., Coyle, J.F., Padgett, K.A., Pagliai, F.A., Gardner, C.L., Lorca, G.L. et al. (2017) Functional characterization of LotP from *Liberibacter asiaticus*. *Microbial Biotechnology*, 10, 642–656.

McCallum, M., Burrows, L.L. & Howell, P.L. (2019) The dynamic structures of the type IV pilus. *Microbiology Spectrum*, 7, 7.2.02.

Melamed, S., Zhang, A., Jarnik, M., Mills, J., Silverman, A., Zhang, H. et al. (2023) σ28-dependent small RNA regulation of flagella biosynthesis. *eLife*, 12, RP87151.

Minamino, T. & Imada, K. (2015) The bacterial flagellar motor and its structural diversity. *Trends in Microbiology*, 23, 267–274.

Morimoto, Y.V. & Minamino, T. (2014) Structure and function of the bi-directional bacterial flagellar motor. *Biomolecules*, 4, 217–234.

Morimoto, Y.V., Nakamura, S., Kami-ike, N., Namba, K. & Minamino, T. (2010) Charged residues in the cytoplasmic loop of MotA are required for stator assembly into the bacterial flagellar motor. *Molecular Microbiology*, 78, 1117–1129.

Nazaret, F., Alloing, G., Mandon, K. & Frendo, P. (2023) MarR family transcriptional regulators and their roles in plant-interacting bacteria. *Microorganisms*, 11, 1936.

Padgett-Pagliai, K.A., Pagliai, F.A., da Silva, D.R., Gardner, C.L., Lorca, G.L. & Gonzalez, C.F. (2022) Osmotic stress induces long-term biofilm survival in *Liberibacter crescens*. *BMC Microbiology*, 22, 1–16.

Pagliai, F.A., Coyle, J.F., Kapoor, S., Gonzalez, C.F. & Lorca, G.L. (2017) LdtR is a master regulator of gene expression in *Liberibacter asiaticus*. *Microbial Biotechnology*, 10, 896–909.

Pagliai, F.A., Gardner, C.L., Bojilova, L., Sarnegrim, A., Tamayo, C., Potts, A.H. et al. (2014) The transcriptional activator LdtR from 'Candidatus *Liberibacter asiaticus*' mediates osmotic stress tolerance. *PLoS Pathogens*, 10, e1004101.

Paul, K., Nieto, V., Carlquist, W.C., Blair, D.F. & Harshey, R.M. (2010) The c-di-GMP binding protein YcgR controls flagellar motor direction and speed to affect chemotaxis by a "backstop brake" mechanism. *Molecular Cell*, 38, 128–139.

Pilizota, T., Brown, M.T., Leake, M.C., Branch, R.W., Berry, R.M. & Armitage, J.P. (2009) A molecular brake, not a clutch, stops the *Rhodobacter sphaeroides* flagellar motor. *Proceedings of the National Academy of Sciences of the United States of America*, 106, 11582–11587.

Platzer, J., Sterr, W., Hausmann, M. & Schmitt, R. (1997) Three genes of a motility operon and their role in flagellar rotary speed variation in *Rhizobium meliloti*. *Journal of Bacteriology*, 179, 6391–6399.

Porter, S.L., Wadhams, G.H., Martin, A.C., Byles, E.D., Lancaster, D.E. & Armitage, J.P. (2006) The CheYs of *Rhodobacter sphaeroides*. *Journal of Biological Chemistry*, 281, 32694–32704.

Py, B., Loiseau, L. & Barras, F. (2001) An inner membrane platform in the type II secretion machinery of gram-negative bacteria. *EMBO Reports*, 2, 244–248.

Rotter, C., Mühlbacher, S., Salamon, D., Schmitt, R. & Scharf, B. (2006) Rem, a new transcriptional activator of motility and chemotaxis in *Sinorhizobium meliloti*. *Journal of Bacteriology*, 188, 6932–6942.

Roujeinikova, A. (2008) Crystal structure of the cell wall anchor domain of MotB, a stator component of the bacterial flagellar motor: implications for peptidoglycan recognition. *Proceedings of the National Academy of Sciences*, 105, 10348–10353.

Roure, S., Bonis, M., Chaput, C., Ecobichon, C., Mattox, A., Barrière, C. et al. (2012) Peptidoglycan maturation enzymes affect flagellar functionality in bacteria. *Molecular Microbiology*, 86, 845–856.

Samsudin, F., Ortiz-Suarez, M.L., Piggot, T.J., Bond, P.J. & Khalid, S. (2016) OmpA: a flexible clamp for bacterial cell wall attachment. *Structure*, 24, 2227–2235.

Santiveri, M., Roa-Eguiara, A., Kühne, C., Wadhwa, N., Hu, H., Berg, H.C. et al. (2020) Structure and function of stator units of the bacterial flagellar motor. *Cell*, 183, 244–257.e16.

Sarkar, M.K., Paul, K. & Blair, D. (2010) Chemotaxis signaling protein CheY binds to the rotor protein FliN to control the direction of flagellar rotation in *Escherichia coli*. *Proceedings of the National Academy of Sciences of the United States of America*, 107, 9370–9375.

Scharf, B. (2002) Real-time imaging of fluorescent flagellar filaments of *Rhizobium lupini* H13-3: flagellar rotation and pH-induced polymorphic transitions. *Journal of Bacteriolology*, 184, 5979–5986.

Scharf, B.E., Hynes, M.F. & Alexandre, G.M. (2016) Chemotaxis signaling systems in model beneficial plant–bacteria associations. *Plant Molecular Biology*, 90, 549–559.

Sobe, R.C., Gilbert, C., Vo, L., Alexandre, G. & Scharf, B.E. (2022) FliL and its paralog MotF have distinct roles in the stator activity of the *Sinorhizobium meliloti* flagellar motor. *Molecular Microbiology*, 118, 223–243.

Sourjik, V., Muschler, P., Scharf, B. & Schmitt, R. (2000) VisN and VisR are global regulators of chemotaxis, flagellar, and motility genes in *Sinorhizobium* (*Rhizobium*) *meliloti*. *Journal of Bacteriology*, 182, 782–788.

Tachiyama, S., Chan, K.L., Liu, X., Hathroubi, S., Peterson, B., Khan, M.F. et al. (2022) The flagellar motor protein FliL forms a scaffold of circumferentially positioned rings required for stator activation. *Proceedings of the National Academy of Sciences of the United States of America*, 119, e2118401119.

Terashima, H., Kawamoto, A., Morimoto, Y.V., Imada, K. & Minamino, T. (2017) Structural differences in the bacterial flagellar motor among bacterial species. *Biophysics and Physicobiology*, 14, 191–198.

Teufel, F., Almagro Armenteros, J.J., Johansen, A.R., Gíslason, M.H., Pihl, S.I., Tsirigos, K.D. et al. (2022) SignalP 6.0 predicts all five types of signal peptides using protein language models. *Nature Biotechnology*, 40, 1–3.

Tsang, J. & Hoover, T.R. (2014) Themes and variations: regulation of RpoN-dependent flagellar genes across diverse bacterial species. *Scientifica*, 2014, 1–14.

Van Way, S.M., Hosking, E.R., Braun, T.F. & Manson, M.D. (2000) Mot protein assembly into the bacterial flagellum: a model based on mutational analysis of the *motB* gene. *Journal of Molecular Biology*, 297, 7–24.

Wadhwa, N. & Berg, H.C. (2022) Bacterial motility: machinery and mechanisms. *Nature Reviews in Microbiology*, 20, 161–173.

Zatakia, H.M., Arapov, T.D., Meier, V.M. & Scharf, B.E. (2018) Cellular stoichiometry of methyl-accepting chemotaxis proteins in *Sinorhizobium meliloti*. *Journal of Bacteriology*, 200, e00614-00617.

Zhou, X. & Roujeinikova, A. (2021) The structure, composition, and role of periplasmic stator scaffolds in polar bacterial flagellar motors. *Frontiers in Microbiology*, 12, 639490.

Zhu, S., Takao, M., Li, N., Sakuma, M., Nishino, Y., Homma, M. et al. (2014) Conformational change in the periplamic region of the flagellar stator coupled with the assembly around the rotor. *Proceedings of the National Academy of Sciences of the United States of America*, 111, 13523–13528.

## SUPPORTING INFORMATION

Additional supporting information can be found online in the Supporting Information section at the end of this article.

**How to cite this article:** Sobe, R.C. & Scharf, B.E. (2024) The swimming defect caused by the absence of the transcriptional regulator LdtR in *Sinorhizobium meliloti* is restored by mutations in the motility genes *motA* and *motS*. *Molecular Microbiology*, 121, 954–970. Available from: https://doi.org/10.1111/mmi.15247